XXI IMEKO World Congress "Measurement in Research and Industry"
August 30 - September 4, 2015, Prague, Czech Republic

Numerical prediction of the flow rate through a flow meter with uncertain inflow profile

A. Weissenbrunner[1], A. Fiebach [1], S. Schmelter[1], M. Straka[1], M. Bär[1], T. Lederer[1]

[1] Physikalisch-Technische Bundesanstalt (PTB), Institut Berlin, Abbestr. 2-12, 10587 Berlin, Germany

Abstract - Flow conditions in industrial pipe and district heating systems are not ideal. Moreover nearly all types of flow measurement devices are sensitive to flow conditions at their inlet section. In this contribution the generalized polynomial chaos method (gPC) is used to study the influence of a disturbed inlet profile with swirl and asymmetry components through a single beam ultrasonic flow meter. This approach allows to estimate the expected variations of the measured volume flow as a function of the position and orientation of the modeled meter in an efficient way.

Keywords: CFD, non-intrusive gPC, uncertainty quantification, flow measurement, disturbed inflow profile

1. Introduction

Industrial pipe and district heating systems consist of assemblies of bends, headers, convergent or divergent pipe sections. Among the different pipe combinations, double bends are of special interest, since they introduce strong disturbances into the flow profile and are the most common installation. Such disturbed velocity profiles decay only after more than 100 diameters behind the installations [17, 10, 7, 15] and can lead to meter errors of several percent as stated in [9, 3] and the references therein. The measured flow rate is dependent on the velocity profile. Therefore every disturbance of the profile causes an error in the volume flow measurement. Since the upstream conditions are unknown in general, an uncertainty investigation is necessary. A variation of the inlet profile in terms of swirl and asymmetry components has to be included in the inflow conditions of the flow meter. To quantify the uncertainty in the flow rate after a bend, a generalized polynomial chaos method is used in conjunction with a commercial deterministic CFD code. The distance between the double bend and the flow meter as well as the orientation of the flow meter are the parameters with the srongest influence on the flow. Therefore, they are considered as random variables in the polynomial chaos approach.

2. Generalized Polynomial Chaos

Generalized polynomial chaos (gPC) plays an important role when dealing with uncertainties [5, 4]. The approach was introduced by N. Wiener [11] and was generalized in [13]. The idea is to expand random variables with a finite second moment in a series of orthogonal polynomials. In contrast to standard Monte-Carlo type methods, the advantage of this approach lies in its speed of performance. In this section we briefly review the gPC method, see [1, 6].

Let $(\Omega, \mathcal{F}, P)$ be a probability space consisting of a σ-algebra $\mathcal{F}$ over the event space Ω and an associated probability measure P. Independent random variables $\xi = (\xi_i)_{i=1}^m$, $m \in \mathbb{N}$, mapping from $(\Omega, \mathcal{F}, P)$ to $(\mathbb{R}^m, \mathcal{B}^m, P_\xi)$ are considered, where $\mathcal{B}$ denotes the Borel σ-algebra and P_ξ denotes the range measure of ξ. Assuming that $\mathcal{F}$ is generated by ξ, every squared integrable mapping $g : (\Omega, \mathcal{F}, P) \to (\mathbb{R}^N, \mathcal{B}^N, P_g)$ can be expanded in series of orthogonal polynomials

$$g(\xi) = \sum_{i=0}^{\infty} \hat{g}_i \Psi_i(\xi), \tag{1}$$

where $(\Psi_i)_{i=0}^{\infty}$ is a family of polynomials, which are orthogonal with respect to the weighted inner product

$$\langle \Psi_i, \Psi_j \rangle_w := \int_{\mathbb{R}^m} \Psi_i(s)\Psi_j(s)w(s)\, ds, \quad i \neq j,$$

with positive weight function w. For simplicity we assume orthonormality: $\langle \Psi_i, \Psi_j \rangle_w = \delta_{ij}$ for $i \neq j$, where δ_{ij} denotes the Kronecker delta function, i.e., $\delta_{ij} = 1$ if $i = j$ and $\delta_{ij} = 0$ if $i \neq j$. The family of the orthogonal polynomials and the probability density function of ξ_i, $i = 1, \ldots, m$, are connected by the Askey scheme, see [13] and Table 1. Using $\Psi_0 = 1$ and the orthogonality of the ansatz,

Distribution	Orthogonal polynomials
Gauss	Hermite
Gamma	Laguerre
Beta	Jacobi
Uniform	Legendre

Table 1. Correspondence of the family of orthogonal polynomials to the type of the probability density function of the random variable. Note that most of the random variables must be scaled in a suitable way such that the corresponding probability density function is equal to the weight function of the polynomial family

the expectation $\mathbb{E}(g)$ and the variance $\mathbb{V}(g)$ are given by

$$\mathbb{E}(g) = \hat{u}_0,$$
$$\mathbb{V}(g) = \mathbb{E}(g^2) - \mathbb{E}(g)^2 = \sum_{i=1}^{\infty} \hat{g}_i^2.$$

The gPC expansion of a random variable can be used to express the solution of an abstract physical system $L(g(x,\xi),\xi) = 0$, $x \in D \subset \mathbb{R}^d$, $d \in \mathbb{N}$. Due to the randomness of ξ, the solution of L becomes a random field over the probability space $(\mathbb{R}^m, \mathcal{B}^m, P_\xi)$ rather than a solution over the spatial space D. Exploiting the orthogonality of the ansatz functions, the modes $\hat{g}_i$ of the series expansion are given by

$$\hat{g}_i(x) = \langle g(x,\cdot), \Psi_i \rangle_w, \quad i = 1, \ldots, \infty. \tag{2}$$

In practical computations, the degree d of the polynomials has to be restricted, which leads to an approximation

$$g(\xi) = \sum_{i=0}^{p} \hat{g}_i \Psi_i(\xi), \quad p+1 = \frac{(d+m)!}{d!m!}, \tag{3}$$

of the series (1). Note that the series increases very fast with the polynomial degree d and the dimension of the random space m. The convergence of the truncated series (3) mainly depends on the polynomial approximation of the solution of the operator L with respect to ξ. In many applications, there exists a well tested and robust numerical solver for the operator L.

Therefore, if the projection $\hat{g}_i$ of g onto Ψ_i in (2) is approximated by a cubature rule

$$\hat{g}_i(x) \approx \sum_{j=1}^{q} g(x,\xi^j)\Psi_i(\xi^j)\lambda^j, \; q \in \mathbb{N}, \tag{4}$$

with nodes $(\xi^j)_{j=1}^q$ and weights $(\lambda^j)_{j=1}^q$, the deterministic solver can still be used for the evaluation of the problem at the nodal points. Here the natural choice is a tensor Gauss cubature formula with suitable weights depending on the weight function w of the orthogonal polynomials.

3. Numerical modeling

The stationary incompressible Navier-Stokes equations modeling conservation of mass and momentum are given by

$$\nabla \cdot u = 0, \qquad u \cdot \nabla u = -\frac{1}{\rho}\nabla p + \nu \Delta u. \tag{5}$$

Here, $u = (u_r, u_\varphi, u_z)^T$ is the velocity field with radial, angular, and axial component, p the pressure, ρ the density of the fluid, and ν its kinematic viscosity. Note that the positions in the pipe geometry are described by cylindrical coordinates (r, φ, z). We prescribe standard no-slip boundary conditions on the walls and a zero-gradient boundary condition at the outlet. At the inlet a fully developed profile with associated turbulence data is used as natural inflow boundary condition. The turbulent flow of water in a pipe of diameter $D = 55\,\text{mm}$ is considered. The pipe behind the double bend has a length of $100\,D$. The geometry of the setup is shown in Figure 1. The volumetric velocity is given by $U_{vol} = 4.19\,\text{ms}^{-1}$, which corresponds to a Reynolds number of about $\text{Re} = 3 \cdot 10^5$.

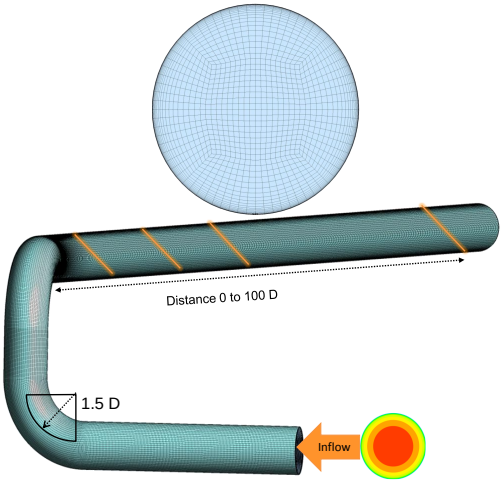

Fig. 1. Top: the generated O-grid at the inlet, bottom: geometric set up of the test case: an out-of-plane double bend with a radius of $1.5D$ along the centerline and fully developed inflow conditions

The numerical simulations of the turbulent flow through such a pipe are performed by ANSYS CFX in three dimensions. Turbulence is modeled by Reynolds-averaging the Navier-Stokes equations (5) and applying the well-known standard k-ω-model, see [12]. For the simulations a hexahedral mesh consisting of 3.2 million elements with a non-dimensional wall distance $y^+ \approx 1$ is used. The mesh was created using the O-grid technique with the tool ANSYS ICEMCFD, see Figure 1 at the top.

4. Measurement principle

Several types of ultrasonic flow meters (USFM) exist on the market. The two main measurement principles are the Doppler and the travel-time techniques. Here, the dual sensor travel-time technique will be discussed. This principle is depicted in Figure 2.

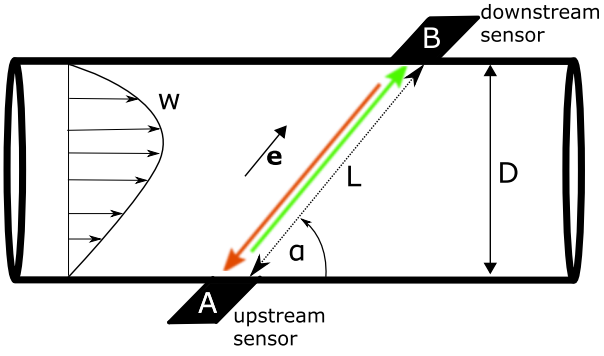

Fig. 2. Measurement principle of a single beam ultra sonic flow meter

Two sensors (A and B) are situated inside or outside the pipe wall. Each sensor is sending and receiving ultrasonic impulses that are propagated through the fluid.

The time between sending and receiving from one to the other sensor is measured. It can be written as:

$$t_{AB} = \frac{L}{C + \bar{U}_p/e_z},\ t_{BA} = \frac{L}{C - \bar{U}_p/e_z}$$

where C denotes the speed of sound in the fluid, $\bar{U}_p$ is the mean velocity along the ultrasonic path and $e_z = \cos(\alpha)$ the z-component of the unit vector $\boldsymbol{e}$ tangential to the path. The measurement value $\bar{U}_p$ is determined by the difference of the times t_{AB} and t_{BA}

$$\bar{U}_p = \frac{L}{2e_z}\left(\frac{1}{t_{AB}} - \frac{1}{t_{BA}}\right).$$

More complex models can be derived such as ray theory path, where the trails of the ultrasonic waves are also depending on the flow conditions. The considered straight line wave propagation is suitable for Mach numbers < 0.1, as mentioned in [16]. Since the mean velocity of a path is not the same as the mean velocity over the cross section, $\bar{U}_p$ has to be multiplied by a calibration factor $k = U_{vol}/\bar{U}_p$, see [2]. The real flow profile in a pipe system is unknown, therefore the ratio k is calculated for a fully developed flow profile. If the flow profile is disturbed particularly not rotationally symmetric, the assumption for k is violated, which depicts the first source of error. The second one is caused by non axial/cross velocity components, because the ultrasonic impulse is not only driven by the axial velocity component u_z. The angle α (practically) cannot be zero, thus the angular cross component u_r is also affecting the measurement value. The measured velocity is then assembled by the scalar product $\boldsymbol{eu}$ with the normalized direction vector

$$\boldsymbol{e} = \begin{pmatrix}\sin(\alpha) & 0 & \cos(\alpha)\end{pmatrix}.$$

Since the axial velocity component u_z is solely inducing the flow rate, an error of the measurement value is expected by huge cross components, such as flows with swirl which occur downstream an out of plane double bend.

5. Application of gPC to flow measurements

In the following, the approach of Section 2 is used to study the influence of a disturbed inflow profile through a non-intrusive single beam ultrasonic meter, which is highly dependent on the flow profile, see [8]. The introduced measurement principle of an single beam ultrasonic meter is modeled in the CFD system. Due to its behavior, the asymmetry and swirl of the velocity profile lead to errors on the measurement values. In order to characterize the influence of the flow profile on the measured volume flow, the location and the angle of the modeled meter is assumed to be random. Thus two uniformly distributed random variables are introduced modeling the distance to the bends $dz = z/D \in [0, 100]$ and the angle $\Phi \in [0, 2\pi]$ of the meter. The axial angle α is fixed by $\pi/4$, see Figure 2 and Figure 3. In order to calculate the modes (2) we use a tensor Legendre-Gauss quadrature rule. The modeled meter is placed at the positions and angles given by the nodes of the cubature rule (4).

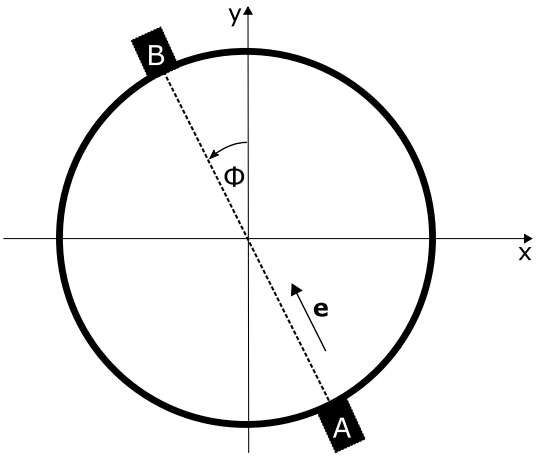

Fig. 3. The random alignment of the circumferential angle Φ of the ultrasonic sensors

6. Results

The development of the velocity profile downstream of an out-of-plane double bend was simulated. The profile has a varying asymmetric shape with swirl which decreases further downstream, see Figure 4. Right after the bend we see a typical sickle-shaped profile. The iso-surface representing the maximum velocity rotates in the flow due to the swirl introduced by the double bend. Further downstream, the profile with the varying asymmetric shape and swirl decreases, see Figure 4 bottom. Such a strongly disturbed (swirl and asymmetry) profile is common in most field installations. The swirl angle is defined by

$$S_a = \arctan\left(\max\left(\sqrt{{u_r}^2 + {u_\varphi}^2}\right)/U_{vol}\right),$$

compare [14]. It represents a measure for the deviation of the velocity vector to the ideal axial direction. The decay of the swirl angle over the position in axial direction downstream the double bend is depicted in Figure 5. In a downstream distance of $40D$ we still have a swirl angle of $5.5°$.

The expected error of the measured flow rate Q_m with random position and random angular alignment of the USFM, compared to the real flow rate Q_{real} is calculated to be $-1.42\,\%$. Since the relative error is given by $100\,(Q_m - Q_{real})\,/Q_{real}$ a negative sign denotes that the measurement value is lower than the real value. This value does not seem very high at first glance. A look at the devolution over the distance shows an asymptotic approximation of the expected error from -4% towards zero. The standard deviation resulting from the variation of the angle Φ on each position is decreasing from 2.5% to 0.5%. The maximum error reaches more than -10% in about 10 diameters distance and still depicts -6% in a distance of $40D$.

In Figure 6 the expected error of the volume flow measured by an ultrasonic single beam over the position of the beam further downstream the double bend is shown. The red error bars represent the standard deviation for

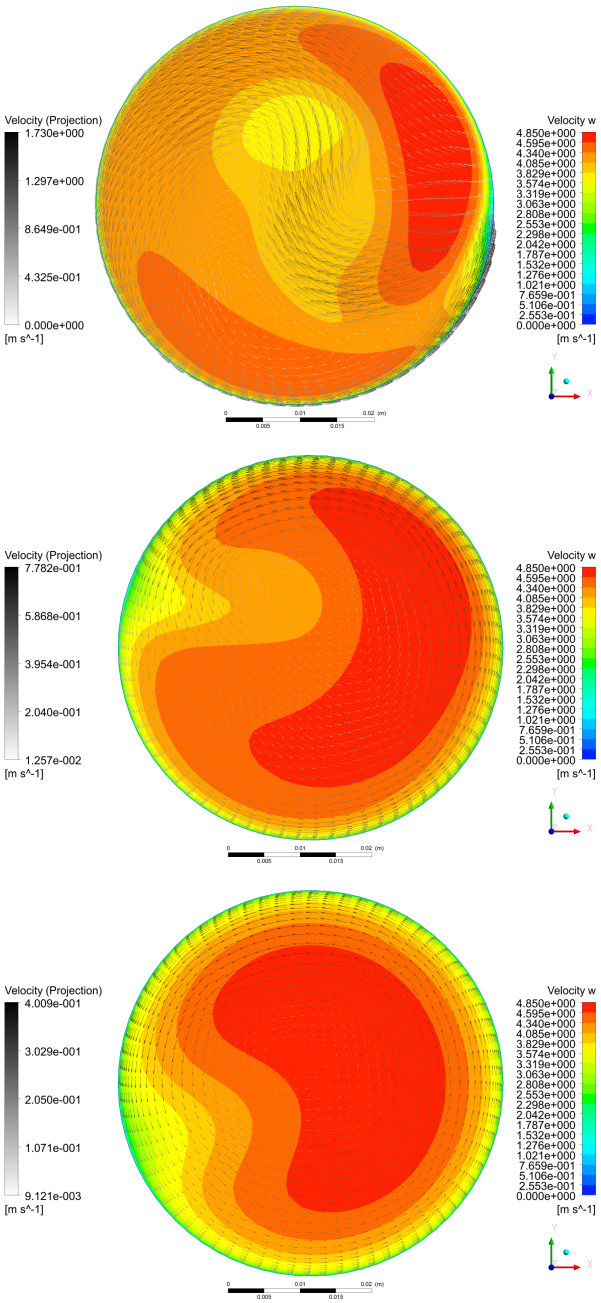

Fig. 4. Contour of the velocity in the axial flow direction 0, $10D$, and $40D$ downstream the double bend. The arrows represent the cross flow components.

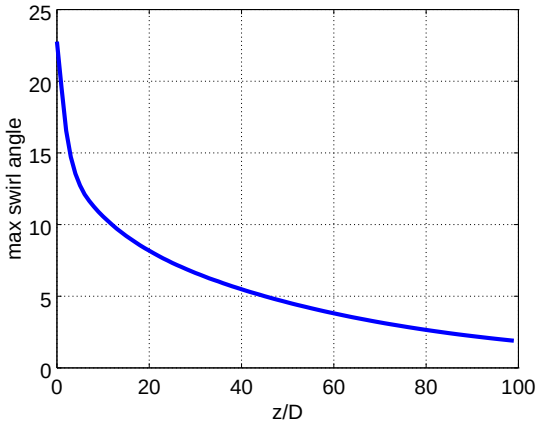

Fig. 5. Decay of the swirl angle S_a over the position z/D downstream the double bend

the angle of the beam. The blue error bars depict the minimum and maximum difference to the expectation value obtained for the different angles. The considered single path ultrasonic measurement is decreasingly sensitive to the disturbed profile. Moreover if the measurement is done closely behind the double bend, it is strongly influenced by the angle.

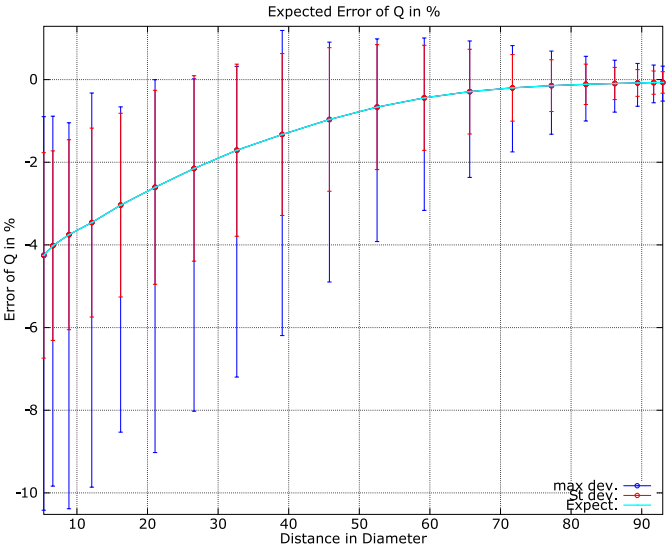

Fig. 6. Development of the expected error (cyan), its standard deviation (red) and the maximum deviation (blue) of a simulated single beam ultrasonic measurement over its position downstream a double bend

7. Conclusion

In this contribution the measurement uncertainty of a single beam ultrasonic flow meter caused by a disturbed flow profile which are usually present under field conditions is considered. The uncertainty was characterized by its mean

and variance. We emphasize the importance to consider disturbed profiles rather than ideal flow profiles for flow measurements.

Moreover, it was demonstrated that gPC is an efficient approach to treat flow problems with random input parameters. Due to its connection to generalized Fourier series, it is easy to apply. The drawback of the method is the curse of dimensionality especially when dealing with problems in a high-dimensional random space. However in the case of computationally expensive problems arising in CFD, the gPC approach is an efficient alternative to the Monte Carlo approach.

ACKNOWLEDGMENTS

The work is partially supported by the European Commission and EURAMET within the EMRP NEW-04 project "Novel mathematical and statistical approaches to uncertainty evaluation".

REFERENCES

[1] F. Augustin, P. Rentrop, and U. Wever. Wiener calculus for differential equations with uncertainties. In M. Günther, A. Bartel, M. Brunk, S. Schöps, and M. Striebel, editors, *Progress in Industrial Mathematics at ECMI 2010*, volume 17 of *Mathematics in Industry*, pages 271–282, Berlin, 2012. The European Consortium for Mathematics in Industry, Springer.

[2] O. Fiedler. *Strömungs- und Durchflußmeßtechnik*. Oldenbourg, München, 1992.

[3] B. Horner and F. Mesch. An induction flowmeter insensitive to asymmetric flow profiles. In M. S. Beck, editor, *Process tomography 1995, 6–8 April 1995, Bergen, Norway*, pages 321–330, Manchester, 1995. UMIST.

[4] S. Hosder, R. W. Walters, and R. Perez. A non-intrusive polynomial chaos method for uncertainty propagation in CFD simulations. In *44th AIAA Aerospace Science Meeting and Exhibit*, Reno, Nevada, 9 – 12 January 2006. American Institute of Aeronautics and Astronautics. AIAA 2006-891.

[5] O. M. Knio and O. P. Le Maitre. Uncertainty propagation in CFD using polynomial chaos decomposition. *Fluid Dyn. Res.*, 38:616–640, 2006.

[6] O. P. Le Maitre and O. M. Knio. *Spectral Methods for Uncertainty Quantification*. Springer, Dordrecht, 2010.

[7] B. Mickan, G. Wendt, R. Kramer, and D. Dopheide. Systematic investigation of pipe flows and installation effects using laser doppler anemometry – part ii. the effect of disturbed flow profiles on turbine gas meters – a describing empirical model. *Flow Meas. Instrum.*, 7:151–160, 1996.

[8] Karsten Tawackolian. *Fluiddynamische Auswirkungen auf die Messabweichung von Ultraschall-Durchflussmessgeräten*. PhD thesis, Technische Universität Berlin, 2013.

[9] G. Wendt. Investigation and characterization of water meter behavior under different flow conditions. *OIML Bulletin*, 55:5–14, 2014.

[10] G. Wendt, B. Mickan, R. Kramer, and D. Dopheide. Systematic investigation of pipe flows and installation effects using laser doppler anemometry -— part i. profile measurements downstream of several pipe configurations and flow conditioners. *Flow Meas. Instrum.*, 7:141–149, 1996.

[11] N. Wiener. The homogeneous chaos. *Amer. J. Math.*, 60:897–936, 1938.

[12] D. C. Wilcox. *Turbulence Modeling for CFD*. DCW Industries, 1994.

[13] D. Xiu and G. E. Karniadakis. The Wiener-Askey polynomial chaos for stochastic differential equations. *SIAM*, 24:1118–1139, 2002.

[14] T. T. Yeh and G. E. Mattingly. Laser doppler velocimeter studies of the pipeflow produced by a generic header. *NIST Technical Note*, 1409:1118–1139, 1995.

[15] T. T. Yeh and G. E. Mattingly. Flowmeter installation effects due to a generic header. Technical Note 1419, National Institute of Standards and Technology, 1996.

[16] T. T. Yeh and G. E. Mattingly. Computer simulations of ultrasonic flow meter performance in ideal and non-ideal pipeflows. *ASME Fluids Engineering Division Summer Meeting FEDSM*, 1997.

[17] H. Zimmermann. Examination of disturbed pipe flow and its effects on flow measurement using orifice plates. *Flow Meas. Instrum.*, 10:223–240, 1999.